Published in final edited form as:
Biomaterials. 2009 August ; 30(23-24): 4037–4046. doi:10.1016/j.biomaterials.2009.04.017.

ON THE R-CURVE BEHAVIOR OF HUMAN TOOTH ENAMEL

Devendra Bajaj[1] and **Dwayne Arola**[1,2,♠]

1 *Department of Mechanical Engineering, University of Maryland Baltimore County, Baltimore, MD 21250*

2 *Department of Endodontics, Prosthodontics, and Operative Dentistry, Baltimore College of Dental Surgery, University of Maryland, Baltimore, MD 21201*

Abstract

In this study the crack growth resistance behavior and fracture toughness of human tooth enamel were quantified using incremental crack growth measures and conventional fracture mechanics. Results showed that enamel undergoes an increase in crack growth resistance (i.e. rising R-curve) with crack extension from the outer to the inner enamel, and that the rise in toughness is function of distance from the Dentin Enamel Junction (DEJ). The outer enamel exhibited the lowest apparent toughness (0.67 ± 0.12 MPa·$m^{0.5}$), and the inner enamel exhibited a rise in the growth toughness from 1.13 MPa·$m^{0.5}$/mm to 3.93 MPa·$m^{0.5}$/mm. The maximum crack growth resistance at fracture (i.e. fracture toughness (K_c)) ranged from 1.79 to 2.37 MPa·m0.5. Crack growth in the inner enamel was accompanied by host of mechanisms operating from the micro- to the nano-scale. Decussation in the inner enamel promoted crack deflection and twist, resulting in a reduction of the local stress intensity at the crack tip. In addition, extrinsic mechanisms such as bridging by unbroken ligaments of the tissue and the organic matrix promoted crack closure. Microcracking due to loosening of prisms was also identified as an active source of energy dissipation. In summary, the unique microstructure of enamel in the decussated region promotes crack growth toughness that is approximately three times that of dentin and over ten times that of bone.

Keywords

Decussation; DEJ; Enamel; Fracture; R-curve; Toughening mechanisms

INTRODUCTION

Enamel, the outermost tissue of the human tooth, serves as a protective enclosure for the dentin and the vital pulp (Fig. 1(a)). Comprised of approximately 96% mineral and only 4% organic matter (1% protein and 3% water) by weight, enamel is the most highly mineralized tissue of the human body [1, 2]. The inorganic portion is largely comprised of carbonated hydroxyapatite in the form of nanometer scale rods (~25 nm thick and ~100 nm wide) that systematically combine to form long ‘keyhole’ shaped structures (4–8 μm in diameter) known as prisms [1, 2]. The prisms are arranged in a parallel fashion and extend from the dentin enamel junction (DEJ) to the occlusal surface. The prisms are surrounded by a ‘sheath’ of non collagenous organic matrix.

♠Corresponding Author Dwayne D. Arola, Ph.D., Department of Mechanical Engineering, University of Maryland Baltimore County, 1000 Hilltop Circle, Baltimore, MD 21250 USA, E-mail: darola@umbc.edu (410) 455-3310 (v) (410) 455-1052 (f).

To support oral function, enamel requires adequate hardness, stiffness and resistance to fracture. As such, the mechanical properties of enamel have been widely studied and discussed in the literature. Due to specimen size constraints imposed by the limited volume of enamel in human teeth, most studies on the mechanical behavior of enamel have been conducted using indentation techniques. The hardness and elastic modulus of enamel measured using indentations range from approximately 3 GPa to 6 GPa [3–5] and 70 GPa to 120 GPa [3–8], respectively. The variation in these properties has mainly been attributed to the structural anisotropy [4] and chemical composition [9,10]. With regards to spatial distribution, both the hardness and elastic modulus increase as a function of distance from the DEJ [8]; the outer (occlusal) enamel exhibits the highest hardness, elastic modulus and brittleness [11].

In comparison to the efforts placed on understanding fracture in dentin and bone, few studies have characterized the fracture behavior of enamel. Rasmussen et al. [12] were the first to quantify crack growth in enamel using a notched (without pre-crack) beam specimen under three point bending. They evaluated the work of fracture (W_f) defined as the work required to form a new surface of unit area. These authors reported that cracks oriented parallel to the prisms required less energy to invoke fracture than those oriented perpendicular to the prisms [12,13]. However, they did not quantify the fracture toughness of enamel.

To date, the “apparent fracture toughness” of enamel has been estimated using indentation fracture resistance only, and varies from 0.4 to 1.5 $MPa{\cdot}m^{0.5}$ [3,11,14,15]. The large range is potentially attributed to the structural anisotropy [3]; enamel exhibits the lowest toughness for cracks oriented parallel to the long axis of the prisms [15]. From a clinical perspective this orientation is of primary interest as natural cracks found *in vivo* are preferentially oriented along the prism axis. With regards to spatial variation, Xu et al. [3] reported higher toughness for cracks in the occlusal surface (0.77 ± 0.05 $MPa{\cdot}m^{0.5}$) compared to that in the buccal or lingual surface (0.52 ± 0.06 $MPa{\cdot}m^{0.5}$). However, other factors such as the magnitude of the indentation load [3,14] and the assumed crack configuration (radial or Palmquist) [16] are important in the measures of indentation fracture resistance. For instance, the apparent toughness estimated assuming a Palmquist crack is reportedly higher than for a radial-median crack [16]. Indentation load may be important as well. Hassan et al. [14] reported an increase in toughness with indentation load, whereas Sakar-Deliormanli and Guden [16] reported a decrease. Perhaps of most relevance, there are several limitations and/or drawbacks to using the indentation approach for estimating fracture toughness [17,18]. After nearly three decades of research there is little consistency in the reported apparent fracture toughness of enamel.

Despite the importance of human enamel to the field of restorative dentistry and the biomaterials community, no reported evaluation has quantified the crack growth resistance of this tissue from incremental crack growth measures coupled with an analysis using traditional fracture mechanics. Therefore, the main objectives of this study were to quantify the fracture toughness of enamel using controlled crack growth experiments and to understand the primary mechanisms contributing to the crack growth resistance. Here we present the first crack growth resistance curves (i.e. R-curves) for human enamel.

MATERIALS AND METHODS

Freshly extracted caries free 3rd molars were acquired from participating dental practices in Maryland according to an approved protocol by the Institutional Review Board of the University of Maryland Baltimore County. The molars were sectioned to obtain small cubes ($2\times2\times2$ mm^3) of cuspal enamel (Fig. 1(a)) using diamond impregnated slicing equipment (K.O. Lee Model S3818EL, Aberdeen, SD, USA) under continuous hydration. Inset compact tension (CT) specimens were prepared by embodying the enamel sections within Vit-l-escence (Ultradent Products, Inc., South Jordan, UT, USA) resin composite with overall dimensions

of 8×6×2 mm^3 (Fig. 1(b)). The methods and equipment used in specimen preparation have been described in detail elsewhere [19, 20]. The inset was placed in the compact tension (CT) specimen body such that the direction of crack growth was oriented along the axis of the prisms. A back channel (1 mm wide) was introduced in all specimens to guide the direction of crack extension. Two holes were counter-bored for application of the opening mode loads as shown in Figure 1(b). Lastly, a chevron notch was machined using a diamond impregnated slicing wheel and the tip was sharpened using a razor blade and diamond paste (1 μm particles) to facilitate crack initiation.

All specimens were subjected to cyclic loading to initiate a crack from the sharpened notch using an Enduratec Model 3200 universal testing system and a hydration bath (22°C) of Hanks Balanced Salt Solution (HBSS). Crack initiation was achieved using a stress ratio (R) of 0.1 and frequency of 5 Hz. Cyclic loading of the specimens was continued until the crack was grown approximately 0.3 mm past the notch, resulting in a total crack length from the load-line of approximately 2 mm (Fig. 1(b)). Thereafter, quasi-static loading of the specimens was performed using a specially designed universal testing system complemented with a microscopic imaging system. A detailed description of the equipment and the imaging system is given elsewhere [20]. Prior to quasi-static loading the specimen surfaces were coated with a very thin layer (approx 5 μm thick) of diluted correction fluid mixed with toner powder (Fig. 2(a)). The coating provided an adequate distribution of fine black speckles on a white background [22] that enabled application of micro Digital Image Correlation (DIC) (Fig. 2(b)). Hydration of the samples during loading was achieved through a saturated cotton swab "cradle" that was nestled beneath the specimen and maintained moist with an eyedropper of HBSS.

Opening mode loads were applied to the CT specimens in 1 Newton increments until the onset of cracking was identified from decay in the load response. Loading was then continued in displacement control (0.1 mm/min) in increments of approximately 0.5 Newtons and lower, followed by a dwell at each load increment, and then followed by partial unloading and reloading. Digital images were acquired using a digital microscope (SMZ-800 Steromicroscope; Nikon, Tokyo, Japan) and CCD camera (CV-A1 CCD camera; JAI America Inc., Laguna Hills, CA) at the onset of loading, at the peak load, and at the end of the load decay to document the crack growth process. The digital images were captured over a field of view of approximately 2×2 mm^2, with a resolution of 1376×1035 pixels. These procedures were followed through progressive increments of crack extension until the onset of instability.

Following the experiments, DIC was performed on the acquired images to determine the full-field displacement distribution within the specimens at selected crack lengths and to identify the crack tip (Fig. 2(b)). A Fast-Search Strategy (FSS) was used in comparing the displacement field of the deformed (i.e. during loading) to the undeformed (before loading) image. The displacement fields were used to examine the crack opening displacement (COD) profile over the entire extension history. In turn, the COD distributions were used to precisely identify the crack tip from the location of "zero" opening displacement in the v-direction (crack opening direction). A detailed description of the DIC process and its application is given elsewhere [20, 22]. The opening mode stress intensity (K_I) distribution with crack extension was calculated according to

$$K_I = \frac{P}{B^* \sqrt{W}} \sqrt{\frac{B^*+1}{B+1}} (1.69 - 8.01\alpha + 12.53\alpha^2) \quad [\text{MPa} \bullet \text{m}^{0.5}] \tag{1}$$

where P is the opening load (Newtons), α is the ratio of a to W (Fig. 1(b)), B is the specimen thickness and B* is the specimen thickness within the back channel. Equation 1 is valid for

$2.0 \leq a \leq 3.6$ mm and was developed from results of a numerical model for fracture. Statistical differences were evaluated using the student's t-test and significance was identified by $p \leq 0.05$.

To understand the mechanisms associated with crack extension, additional microscopic observations of the crack path were performed on uncoated specimens using a digital microscope (Navitar, IEEE 1394). In addition, unbroken and fractured enamel specimens were dehydrated in air for 24 hours, sputtered with gold palladium, and examined using a scanning electron microscope (SEM, model JSM 5600, JEOL Inc., Peabody, MA) in secondary electron imaging mode.

RESULTS

A typical load versus load-line displacement response from quasi static loading is shown in Figure 2(c) and highlights pre-loading (Region I) and incremental crack extension (Region II). For all specimens the initial (i.e. first) crack growth increment extended over a comparatively large distance (Δa_i) $0.3 \sim \Delta a_i \sim 0.8$ mm. Thereafter, the crack growth increments progressed over smaller extensions ($\Delta a_i < 0.1$ mm) until the specimen underwent unstable fracture. An optical micrograph of the crack path within an enamel inset specimen is shown in Figure 3(a). Notice that the crack exhibits two distinct zones with unique morphology. The first half (left) of the incremental crack growth (of Region II) is characterized by a continuous straight path, whereas the second half (right) exhibits a discontinuous path with evidence of crack deflection, crack bifurcation, and a number of fractured ligaments that bridged the crack. However, based on these features, the crack growth responses were characterized in terms of the 'outer' (nearest the tooth's surface) and the 'inner' (nearest the DEJ) enamel. The physical distinction between the outer and inner enamel was further established from observation of the fracture surfaces (Fig. 3(b)). Straight prisms were present in the outer enamel, in contrast to the oblique crossing of bundles of prisms (i.e. decussation) in the inner enamel. Analogous to features observed using optical microscopy, the SEM observation of the fracture surfaces revealed a transition from a smooth fracture plane in the outer enamel (Fig. 3(c)) to a comparatively rough surface in the inner enamel (Fig. 3(d)). These two zones of crack growth were distinctly evident and established that the crack growth resistance was a function of distance from the tooth's surface.

A typical crack growth resistance curve for an enamel specimen is shown in Figure 4(a). All specimens exhibited a rise in critical stress intensity with crack extension (i.e. rising R-curve) as evident in this figure. Overall, the rise in crack growth resistance with crack extension was lowest within the outer enamel and increased with proximity to the DEJ. Crack growth in the innermost enamel was frequently arrested and required higher driving forces to continue extension. The R-curves were quantified in terms of the initiation and growth behavior, which corresponded to growth within the outer and inner regions, respectively. Specifically, the magnitude of stress intensity at the onset of stable crack extension from the existing pre crack was quantified by the "initiation toughness" (K_o) as denoted in Figure 4(a). For most materials that exhibit rising R-curve behavior the fracture toughness (K_c) is quantified from the "plateau[†]" in fracture resistance [23]. However, the enamel responses did not exhibit a distinct plateau and, hence, the K_c was quantified from the maximum recorded stress intensity (K_I) at the onset of unstable fracture. The rise in resistance with incremental extension between K_o and K_c was quantified by a "growth toughness" (K_g) defined by the slope of the stress intensity distribution per unit crack extension. Note that K_g was quantified for the outer and the inner enamel separately according to the crack location. The maximum growth toughness in the inner enamel ($K_{g(i)}$) was estimated from the slope of a second degree polynomial fit to the growth

[†]The plateau toughness is identified from the region where there is no further increase in the critical stress intensity with crack extension. In most cases, the plateau toughness is achieved after full development of the extrinsic zone.

response (Fig. 4(a)) near the point of instability. Crack growth resistance curves for stable extension (up to approximately 1.6 mm) in all the enamel specimens are shown in Figure 4(b).

The specific components of toughness obtained from the R-curves are listed in Table 1. The initiation toughness ranged from 0.52 MPa·$m^{0.5}$ to 0.83 MPa·$m^{0.5}$ (avg = 0.67±0.12 MPa·$m^{0.5}$) and the fracture toughness ranged from 1.79 MPa·$m^{0.5}$ to 2.37 MPa·$m^{0.5}$ (average = 2.07±0.22 MPa·$m^{0.5}$). The average K_g for the outer enamel ($K_{g(o)}$ = 0.11±0.18 MPa·$m^{0.5}$/mm) was significantly lower ($p<0.002$) than that for the inner enamel ($K_{g(i)}$ = 2.62±1.39 MPa·$m^{0.5}$/mm). The pooled response for enamel was also evaluated where the data from all specimens was combined to form a single response; the pooled data resulted in a K_o of 0.68 MPa·$m^{0.5}$, K_c of 2.04 MPa·$m^{0.5}$ and growth toughness within the outer and inner enamel of 0.03 MPa·$m^{0.5}$/mm and 1.3 MPa·$m^{0.5}$/mm, respectively. Results from both assessments distinguished that the largest rise in crack growth resistance occurred in the inner enamel (especially in proximity of the DEJ) and that the largest resistance was always consistent with the point of instability.

The rise in crack growth resistance was accompanied by a number of mechanisms that appeared to be restricted to the inner (decussated) enamel. Crack bridging induced by unbroken ligaments was evident from examination of the advancing crack (Fig. 3(a)). From observations of the crack path and the ligaments it appeared that the bridging material was comprised of prisms as well as interprismatic enamel. Observations of the crack face at high magnification also showed evidence of bridging induced by the organic matrix residing between the prisms (Fig. 5). The fracture surfaces showed evidence of broken ligaments spread across the specimen thickness, as well as complex crack growth patterns that coincided with the unique arrangement of prisms (Fig. 6). A schematic representation of prism decussation is shown in Figure 6(a). In the outer enamel with relatively straight prisms the crack extended along the weaker prism boundaries as evident by the dome-shaped prism heads appearing about the fracture plane (Fig. 6(b)). Within the inner enamel, the crack frequently encountered prisms oblique to the crack path, causing either in-plane deflection (twist) up to 45° (Fig. 6(c)) or out of plane deflection (curving) up to 70° (Fig. 3(d)). In such cases the crack extended both along and across the prisms, resulting in fracture of the prisms rods (Fig. 6(d)) as well as pullout and fracture of the nano crystallites within the intraprismatic enamel (Fig. 6(e)). In addition, cracks traversing from the outer enamel into the decussated region encountered interprismatic regions ahead of the crack tip running oblique (in some regions perpendicular) to the crack plane resulting in loosening (microcracking) along the prism boundaries.

DISCUSSION

An evaluation of the fracture behavior of human enamel was conducted from incremental crack growth measurements and a corresponding analysis using traditional fracture mechanics. Results showed that enamel exhibits rising R-curve behavior and that the crack growth resistance is a function of distance from the DEJ. The outer enamel exhibited the lowest resistance with K_o = 0.67 MPa·$m^{0.5}$ and growth toughness ($K_{g(o)}$) of 0.11 MPa·$m^{0.5}$/mm. A marked rise in toughness ensued when the crack reached the decussated zone; the average growth resistance increased to $K_{g(i)}$ of 2.62 MPa·$m^{0.5}$/mm. The fracture toughness (K_c), quantified from the maximum critical stress intensity, ranged from 1.79 to 2.37 MPa·$m^{0.5}$ (avg = 2.07±0.22 MPa·$m^{0.5}$). The values of K_o, K_g and K_c reported here are the first measures of toughness for enamel obtained from a crack growth resistance curve. Overall, the initiation toughness is within the range of toughness reported using indentation techniques (0.44 – 0.9 MPa·$m^{0.5}$) [3,15,24]. However, the fracture toughness is more than twice the estimates obtained from indentation fracture resistance measurements.

Interestingly, the outer enamel (Fig. 4) offered minimal rise in the crack growth resistance with extension and essentially a "flat" R-curve response. The initiation toughness defined at the onset of growth is within 10% of the toughness of monolithic hydroxyapatite (0.6 $MPa{\cdot}m^{0.5}$) [25]. From a mechanistic point of view both hydroxyapatite and the outer enamel lack the microstructural features that dissipate fracture energy like that within the decussated region. There appears to be functional significance to this behavior: enamel guides surface cracks through the region of straight prisms in the outer enamel towards the inner regions. This guided crack growth prevents chipping of enamel, but contains the crack within the tooth. Crack extension into the inner enamel promotes extrinsic toughening that raises the measured growth resistance to over three times that of K_o. The ability to transform from a flat R-curve behavior in the outer enamel to a rising resistance in the inner enamel is a very unique quality, and one that appears unprecedented in evaluations of the crack growth resistance of other hydrated tissues, and especially engineered materials.

Observation of the fracture surfaces revealed distinct mechanisms contributing to the difference in growth resistance between the outer and inner enamel. Crack growth along the straight prisms of the outer enamel was mostly confined to the weak matrix about the interprismatic space as evident from the exposed dome-shaped prism heads raised above the fracture plane (Fig. 6(b)). The rise in crack growth resistance in the inner enamel was associated with a highly tortuous fracture plane (Fig. 3(d)) resulting from meandering of the crack through the decussated enamel. Crack plane deflections up to 70° and twist angles up to 45° were observed, especially in close proximity (~ 500 μm) to the DEJ (Fig. 3(d) and Fig. 6(c)). Such deflections promote a decrease in the local stress intensity at the crack tip that is available to drive fracture. A simple quantitative estimate for the reduction in local stress intensity at the tip of a deflected crack can be obtained using [26]

$$\begin{aligned} k_1 &= a_{11}(\theta)K_I + a_{12}(\theta)K_{II} \\ k_2 &= a_{21}(\theta)K_I + a_{22}(\theta)K_{II} \end{aligned} \tag{2}$$

where k_1 and k_2 are the local stress intensity for the deflected crack and K_I and K_{II} are the far field (or global) stress intensity for the main crack. Coefficients $a_{ij}(\theta)$ are mathematical functions of deflection angle (θ). The effective stress intensity (K_{eff}) at the tip of the deflected crack can be estimated by

$$K_{eff} = \sqrt{k_1^2 + k_2^2} \tag{3}$$

For a 70° crack deflection (from Figure 3(c)), the stress intensity at the crack tip is reduced by over 30%. The stress intensity at the crack tip is further deceased by the combined effect of deflection and twist. The corresponding stress intensity factors (K^T) applicable for crack twist can be expressed as [27]

$$\begin{aligned} K_1^T &= b_{11}(\varphi)k_1 + b_{12}(\varphi)k_2 \\ K_3^T &= b_{31}(\varphi)k_1 + b_{32}(\varphi)k_2 \end{aligned} \tag{4}$$

where K_1^T and K_3^T are the local mode I and mode III stress intensity for the deflected and twisted crack. Coefficients b_{ij} (φ) are angular functions of twist angle (φ) and k_1 and k_2 are the local stress intensities for the deflected crack obtained from Eq. (2). For combined contribution of

deflection and twist (φ= 45°) the stress intensity at the crack tip can be reduced by almost 75%. Note, however, that such crack deflections are not continuous, but scattered across the specimen thickness. This is a formidable problem to approach analytically, and is reserved for future study.

Bridging of the crack by unbroken ligaments of tissue and the organic matrix operating within the inner enamel promoted shielding and further reduced the local stress intensity available to drive fracture. Such mechanisms promote crack closure that requires higher driving forces for continuing crack propagation. Crack bridging has been found to be a significant contributor to the toughness of bone [28] and dentin [29]. First order theoretical estimates of bridging stress intensity induced by the unbroken ligaments comprised of enamel prisms can be obtained using [30]

$$K_{b(prisms)}=\frac{-f_b K_I[(1+\ell_b/rb)^{1/2}-1]}{[1-f_b+f_b(1+\ell_b/rb)^{1/2}]} \quad (5)$$

where f_b is the area fraction of bridging ligaments (~0.8, from observation of crack path), K_I is the applied stress intensity (1.79–2.37 MPa·$m^{0.5}$), ℓ_b is the bridging zone length (~500–700 μm, from observation of crack path), r is the rotational factor (0.20–0.47) [30] and b is the uncracked specimen length (W-a) (Fig. 1(b)) ahead of the crack. Substituting typical values for these parameters in Eq. (5) results in bridging stress intensity that ranges from 0.22 to 0.56 MPa·$m^{0.5}$. These values represent up to approximately 25% of the global estimates of the toughness.

Observation of the advancing crack also suggested the development and participation of secondary ligaments of organic matrix (Fig. 5). While the chemical composition of these bridges was not identified quantitatively, the nonlinear geometry of these bridges and the degree of extension (1 to 2 μm) indicates that they are not highly mineralized. The reduction in the stress intensity associated with bridging by the organic matrix (Fig. 5) can be estimated using the uniform traction Dugdale-zone model [31] defined as

$$K_{b(protein)}=2\sigma_b f_p\left(\frac{2\ell_p}{\pi}\right)^{1/2} \quad (6)$$

where σ_b is the nominal bridging stress on the protein matrix (assumed to be equivalent to the yield strength of protein ~ 20 MPa [32]), f_b is the area fraction of protein matrix bridging ligaments (0.2, from observation of crack path), ℓ_b is the bridging zone length (10–200 μm, from observation of crack path). Substituting typical values for these parameters in Eq. (6) results in a protein bridging stress intensity of ~0.10 MPa·$m^{0.5}$. Contribution of the organic-based bridging to toughening is far less than that of the enamel prisms. However, it is the qualities of the organic matrix that promotes the development of bridging by the enamel prisms. The microstructure encourages crack growth along the path of highest organic content but the toughness does not undergo a substantial increase because of bridging stress posed by the protein. Considering the combination of mineralized ligament and protein induced bridging results in a reduction of the local stress intensity up to ~0.66 MPa·$m^{0.5}$.

The intrinsic toughness of a material represents the inherent resistance to development of new crack surface area without the contribution of a process zone. As there is no physical evidence of extrinsic mechanisms operating in the crack wake in the outer enamel (Fig. 3(a)) the initiation

toughness (K_o) can be used as an estimate of the intrinsic toughness of enamel. The shielding stress intensity (K_s) can then be estimated by subtracting K_o from the estimated critical stress intensity (K_c) at fracture, which gives 1.08 MPa·m0.5 to 1.72 MPa·m0.5. But the total stress intensity estimated for bridging using Eqs. (5) and (6) accounts for less than half of this estimate, suggesting that bridging is not the only toughening mechanism in enamel. Crack tip shielding attributed to microcracking in the inelastic region is also an active energy dissipation mechanism. Brittle materials such as ceramics are toughened by microcracks via dilatation and a moderate reduction in the elastic modulus in the process zone [33]. Enamel may undergo similar toughening through loosening of the prisms. The increase in toughness associated with microcracking (K_m) can be estimated from [33]

$$K_m = 0.22\varepsilon_m E' f_m \sqrt{\ell_m} + \beta f_m K_c \quad (7)$$

where ε_m is the residual volumetric strain (0.002 [34]), E′ is the plane strain elastic modulus (90 GPa [8]), f_m is the volume fraction of microcracks (~15%, from observation of crack path), ℓ_m is the height of the microcrack zone (~20 μm, from crack path observation, [Bajaj and Arola, unpublished results]), β is a factor dependent on Poisson's ratio (~1.2 [34]). Substituting typical values for these parameters in Eq. (7) results in a stress intensity ranging from 0.38 – 0.49 MPa·$m^{0.5}$. The cumulative stress intensity accounting for these mechanisms (Eqs. 5,6 & 7) ranges from 0.7 to 1.15 MPa·$m^{0.5}$. This is a reasonable first order estimate of the contribution from extrinsic mechanisms, but does not account for variability related to changes in the microstructure with distance from the tooth's surface. Contributions from microcracking and as well as protein bridging should increase with depth as the extent of decussation [35] and degree of protein matrix [1] increase with proximity to the DEJ. Energy dissipation can also occur via mechanisms operating at the sub-micron scale. The crystallites comprising a prism rod undergo gradual transition in the orientation from 0° in the prism head to 90° at the tail (interprism). This large deviation in the orientation of these nano-rods aids in energy dissipation via pullout/fracture of crystallites within the prisms (Fig. 6(c)) and potentially shearing of individual or bundles of nano-crystallites [36].

A comparison of results from the present study with those from similar evaluations on bone [28,37] and dentin [38,39] reveals that all hard tissues of the human body exhibit rising R-curve behaviour (Fig. 7). But surprisingly, the tissue with the highest mineral content (i.e. enamel) undergoes the largest degree of toughening per unit crack extension as shown in Table 2. In comparing specific components of toughness, the K_o of enamel (0.67 ± 0.12 MPa·$m^{0.5}$) is significantly less than that of bone (1–2 MPa·$m^{0.5}$) [37] and dentin (1.34 ± 0.06 MPa·$m^{0.5}$) [38], which is not surprising due to the high mineral content. Note, however, that the average growth toughness ($K_{g(i)}$ = 2.62 MPa·$m^{0.5}$/mm) of the inner enamel is approximately three times that of dentin (0.93 MPa·$m^{0.5}$/mm) [38] and more than ten times that of bone (~0.25 MPa·$m^{0.5}$/mm) [37] for comparable lengths of extension (Δa<2 mm). The resulting range of toughness of the inner enamel (1.79 – 2.37 MPa·$m^{0.5}$) is similar to that of bone‡ (1.6 – 2.5 MPa·$m^{0.5}$) [37]. Also, unlike the R-curves for dentin and bone, the enamel response does not achieve a plateau over the physiologically relevant length scale. This finding highlights that there is a continuous growth of the process zone during crack extension in enamel. Saturation of the process zone might only be achieved when the crack penetrates through the DEJ into dentin. It appears that the resistance of the tooth to crack growth is not just limited to the DEJ; the enamel could play an equally important, or perhaps even more important role in resisting tooth fracture. Note that the estimated toughness of enamel (Table 1) falls within the range of

‡The extrinsic zone in bone is not fully developed for short crack lengths (Δa< 2.5 mm). Extrinsic mechanisms are fully evolved for crack growth in the millimetre range (~5 mm) in which case bone exhibits further increase in toughness up to ~ 5 MPa·$m^{0.5}$ [28,40].

apparent toughness measures reported in the literature for the DEJ (0.6 to 3.4 MPa·$m^{0.5}$) [41–44].

Though the most highly mineralized tissue of the human body, human enamel exhibits exceptional resistance to both cyclic [21] and monotonic crack growth. The remarkable resilience of enamel to crack growth surpasses that of many clinical restorative materials. Within the inner enamel the steepest rise in crack growth resistance occurred for enamel that was in the proximity (~500 μm) of the DEJ. The "functional grading" of the DEJ is not limited to the ~10 μm interface joining the enamel and the dentin [45], but extends from the decussated region (~ 500–700 μm) in the inner enamel to the mantle dentin. Results from the present work showed that the key to the crack growth resistance of enamel is the arrangement of prisms in the inner enamel as well as the presence and the distribution of organic matrix. As such, loss of the organic matrix, or replacement with mineral, could be detrimental to the resistance of teeth to fracture.

Recent research efforts have focused on the synthesis of enamel-like restorative materials or the repair of enamel through controlled remineralization [46–48]. Biomineralization processes reported to date have not been able to replicate the decussating structure of enamel. The results presented in this work indicate that the development of 'enamel-like' restorative materials for crown replacement must include the complex microstructure apparent in the inner enamel, or a variation with equivalent benefits. Without this feature, achieving the desired strength without compromising the toughness in such biomimetic materials will be challenging.

CONCLUSIONS

Based on a study of monotonic crack growth in human enamel, the following conclusions were drawn:

1. Enamel exhibits rising R-curve behaviour. The rise in toughness occurs primarily in the inner decussated enamel. A 300% increase in the toughness occurred from initiation (0.67 ± 0.12 MPa·$m^{0.5}$) to fracture (2.07 ± 0.22 MPa·$m^{0.5}$) over less than 1.6 mm of extension. The growth toughness increased with proximity to the DEJ (average growth toughness of 2.62 ± 1.39 MPa·$m^{0.5}$/mm) with values reaching as high as 5.0 MPa·$m^{0.5}$/mm.
2. The rise in crack growth resistance was attributed to several mechanisms of toughening including crack bridging, crack deflection and microcracking. These mechanisms appeared to operate only within the inner enamel. The fracture surfaces revealed that crack growth occurred primarily along the interprismatic boundaries. In regions of acute decussation crack growth was retarded by deflection, twist and fracture through the prisms. Overall, the microstructure of enamel promoted guided crack growth and arrest, resulting in substantial toughening.
3. First order estimates of the reduction in local stress intensity resulting from the dominant mechanisms contributing to the toughness were obtained using reported theoretical models. The reduction in stress intensity induced by unbroken ligament bridges of the tissue ranged from 0.22–0.56 MPa·$m^{0.5}$, whereas that for bridging induced by the organic matrix was ~ 0.10 MPa·$m^{0.5}$. Similarly, first order estimates for the contribution from microcracking (loosening of prisms) ranged from 0.38–0.49 MPa·$m^{0.5}$.

Acknowledgments

This work was supported in part by the NSF (BES0521467) and the NIDCR (DE016904). The authors would like to thank Ultradent Products Inc for supplying the Vit-l-escence resin composite, Dr. Judith Porter of the University of Maryland, Baltimore for technical support regarding bonding practice and Dr. Ahmad Nazari for numerical modelling.

Support for the following investigation was provided by the NSF (BES0521467) and the NIDCR (DE016904)

References

1. Ten Cate, AR. Oral histology: Development, structure and function. Vol. 5. St. Louis; Mosby: 1998. p. 218-221.
2. Robinson, C.; Kirkham, J.; Shore, R. Dental enamel: Formation to destruction. Boca Raton: CRC press; 1995. p. 151-152.
3. Xu HHK, Smith DT, Jahanmir S, Romberg E, Kelly JR, Thompson VP, et al. Indentation damage and mechanical properties of human enamel and dentin. J Dent Res 1998;77:472–480. [PubMed: 9496920]
4. Habelitz S, Marshall SJ, Marshall GW Jr, Balooch M. Mechanical properties of human dental enamel on the nanometer scale. Arch Oral Biol 2001;46:173–183. [PubMed: 11163325]
5. Mann AB, Dickinson ME. Nanomechanics, chemistry and structure at the enamel surface. Monogr Oral Sci 2006;19:105–131. [PubMed: 16374031]
6. Balooch G, Marshall GW, Marshall SJ, Warren OL, Asif SA, Balooch M. Evaluation of a new modulus mapping technique to investigate microstructural features of human teeth. J Biomech 2004;37:1223–1232. [PubMed: 15212928]
7. He LH, Fujisawa N, Swain MV. Elastic modulus and stress-strain response of human enamel by nanoindentation. Biomaterials 2006;27:4388–4398. [PubMed: 16644007]
8. Park S, Wang DH, Zhang D, Romberg E, Arola D. Mechancal properties of human enamel as a function of age and location in the tooth. J Mater Sci Mater Med 2008;19:2317–2324. [PubMed: 18157510]
9. Cuy JL, Mann AB, Livi KJ, Teaford MF, Weihs TP. Nanoindentation mapping of the mechanical properties of human molar tooth enamel. Arch Oral Biol 2002;47:281–291. [PubMed: 11922871]
10. Braly A, Darnell LA, Mann AB, Teaford MF, Weihs TP. The effect of prism orientation on the indentation testing of human molar enamel. Arch Oral Biol 2007;52:856–860. [PubMed: 17449008]
11. Park S, Quinn JB, Romberg E, Arola D. On the brittleness of enamel and selected dental materials. Dent Mater 2008;24:1477–1485. [PubMed: 18436299]
12. Rasmussen ST, Patchin RE, Scott DB, Heuer AH. Fracture properties of human enamel and dentin. J Dent Res 1976;55:154–164. [PubMed: 1060651]
13. Rasmussen ST, Patchin RE. Fracture properties of human enamel and dentin in an aqueous environment. J Dent Res 1984;63:1362–1368. [PubMed: 6595288]
14. Hassan R, Caputo AA, Bunshah RF. Fracture toughness of human enamel. J Dent Res 1981;60:820–827. [PubMed: 6937518]
15. White SN, Luo W, Paine ML, Fong H, Sarikaya M, Snead ML. Biological organization of hydroxyapatite crystallites into a fibrous continuum toughens and controls anisotropy in human enamel. J Dent Res 2001;80:321–326. [PubMed: 11269723]
16. Sakar-Deliormanli A, Guden M. Microhardness and fracture toughness of dental materials by indentation method. J Biomed Mater Res B: Appl Biomater 2006;76:257–264. [PubMed: 16211564]
17. Quinn GD, Bradt RC. On the vickers indentation fracture toughness test. J Am Cer Soc 2007;90:673–680.
18. Quinn GD. Fracture toughness of ceramics by the Vickers indentation crack length method: A critical review. Mechanical Properties and Performance of Engineering Ceramics II: Ceramic Engineering and Science Proceedings 2008;27:45–62.
19. Soappman M, Nazari A, Porter JA, Arola D. A comparison of fatigue crack growth in resin composite, dentin and the interface. Dent Mater 2007;23:608–614. [PubMed: 16806452]
20. Zhang D, Nazari A, Soappman M, Bajaj D, Arola D. Methods for examining the fatigue and fracture behaviour of hard tissues. Exp Mech 2007;47:325–336.

21. Bajaj D, Nazari A, Eidelman N, Arola D. A comparison of fatigue crack growth in enamel and hydroxyapatite. Biomaterials 2008;29:4847–4854. [PubMed: 18804277]
22. Zhang D, Arola D. Application of digital image correlation to biological tissues. J Biomed Opt 2004;9:691–699. [PubMed: 15250755]
23. Anderson, TL. Fracture Mechanics: Fundamentals and Applications. Vol. 3. CRC press; 2005.
24. Marshall GW Jr, Balooch M, Gallagher RR, Gansky SA, Marshall SJ. Mechanical properties of the dentinoenamel junction: AFM studies of nanohardness, elastic modulus, and fracture. J Biomed Mater Res 2001;54:87–95. [PubMed: 11077406]
25. Pezzotti G, Sakakura S. Study of the toughening mechanisms in bone and biomimetic hydroxyapatite materials using Raman microprobe spectroscopy. J Biomed Mater Res A 2003;65:229–236. [PubMed: 12734817]
26. Suresh, S. Fatigue of materials. Vol. 2. Cambridge: Cambridge University Press; 1998.
27. Faber KT, Evans AG. Crack deflection processes-I. Theory Acta Metall 1983;31:565–576.
28. Nalla RK, Kruzic JJ, Kinney JH, Ritchie RO. Mechanistic aspects of fracture and R-curve behavior in human cortical bone. Biomaterials 2005;26:217–231. [PubMed: 15207469]
29. Kruzic JJ, Nalla RK, Kinney JH, Ritchie RO. Crack blunting, crack bridging and resistance-curve fracture mechanics in dentin: effect of hydration. Biomaterials 2003;24:5209–5221. [PubMed: 14568438]
30. Shang JK, Ritchie RO. Crack bridging by uncracked ligaments during fatigue-crack growth in SiC-reinforced aluminum-alloy composites. Metall Trans A 1989;20A:897–908.
31. Evans AG, McMeeking RM. On the toughening of ceramics by strong reinforcements. Acta Metall 1986;34:2434–2441.
32. Ji B, Gao H. Mechanical properties of nanostructure of biological materials. J Mech Phys Solids 2004;52:1963–1990.
33. Evans AG, Faber KT. Crack growth resistance of microcracking brittle solids. J Am Ceramic Soc 1984;84:255–260.
34. Sigl LS. Microcrack toughening in brittle materials containing weak and strong interfaces. Acta Metall 1996;44:3599–3609.
35. Kodaka T, Kuroiwa M, Abe M. Fine structure of the inner enamel in human permanent teeth. Scanning Microsc 1990;4:975–985. [PubMed: 2094013]
36. Xie Z, Swain M, Munroe P, Hoffman M. On the critical parameters that regulate the deformation behaviour of tooth enamel. Biomaterials 2008;29:2697–2703. [PubMed: 18359075]
37. Vashishth D, Behiri J, Bonfield J. Crack growth resistance in cortical bone: Concept of microcrack toughening. J Biomech 1997;30:763–769. [PubMed: 9239560]
38. Nazari A, Bajaj D, Zhang D, Romberg E, Arola D. Aging and the reduction in fracture toughness of dentin. J Mech Behav Biomed Mater. 10.1016/j.jmbbm.2009.01.008
39. Koester KJ, Ager JW 3rd, Ritchie RO. The effect of aging on crack-growth resistance and toughening mechanisms in human dentin. Biomaterials 2008;29:1318–1328. [PubMed: 18164757]
40. Koester KJ, Ager JW 3rd, Ritchie RO. The true toughness of human cortical bone measured with realistically short cracks. Nat Mater 2008;7:672–677. [PubMed: 18587403]
41. White SN, Paine ML, Wen L, Sarikaya M, Fong H, Zhaokun Y, et al. The dentino-enamel junction is a broad transitional zone uniting dissimilar bioceramic composites. J Am Ceram Soc 2000;83:238–240.
42. Lin CP, Douglas WH. Structure-property relations and crack resistance at the bovine dentin-enamel junction. J Dent Res 1994;73:1072–1078. [PubMed: 8006234]
43. Dong XD, Ruse ND. Fatigue crack propagation path across the dentinoenamel junction complex in human teeth . J Biomed Mater Res 2003A;66:103–109.
44. Imbeni V, Kruzic JJ, Marshall GW, Marshall SJ, Ritchie RO. The dentin-enamel junction and the fracture of human teeth. Nat Mater 2005;4:229–232. [PubMed: 15711554]
45. Habelitz S, Marshall SJ, Marshall GW, Balooch M. The functional width of the DEJ determined by AFM-based nanoscratching. J Struct Biol 2001;135:244–301.
46. Chen H, Clarkson BH, Sun K, Mansfield JF. Self-assembly of synthetic hydroxyapatite nanorods into an enamel prism-like structure. J Colloid Interface Sci 2005;288:97–103. [PubMed: 15927567]

47. Palmer LC, Newcomb CJ, Kaltz SR, Spoerke ED, Stupp SI. Biomimetic systems for hydroxyapatite mineralization inspired by bone and enamel. Chem Rev 2008;108:4754–4783. [PubMed: 19006400]

48. Fan Y, Sun Z, Moradian-Oldak J. Controlled remineralization of enamel in the presence of amelogenin and fluoride. Biomaterials 2009;30:478–483. [PubMed: 18996587]

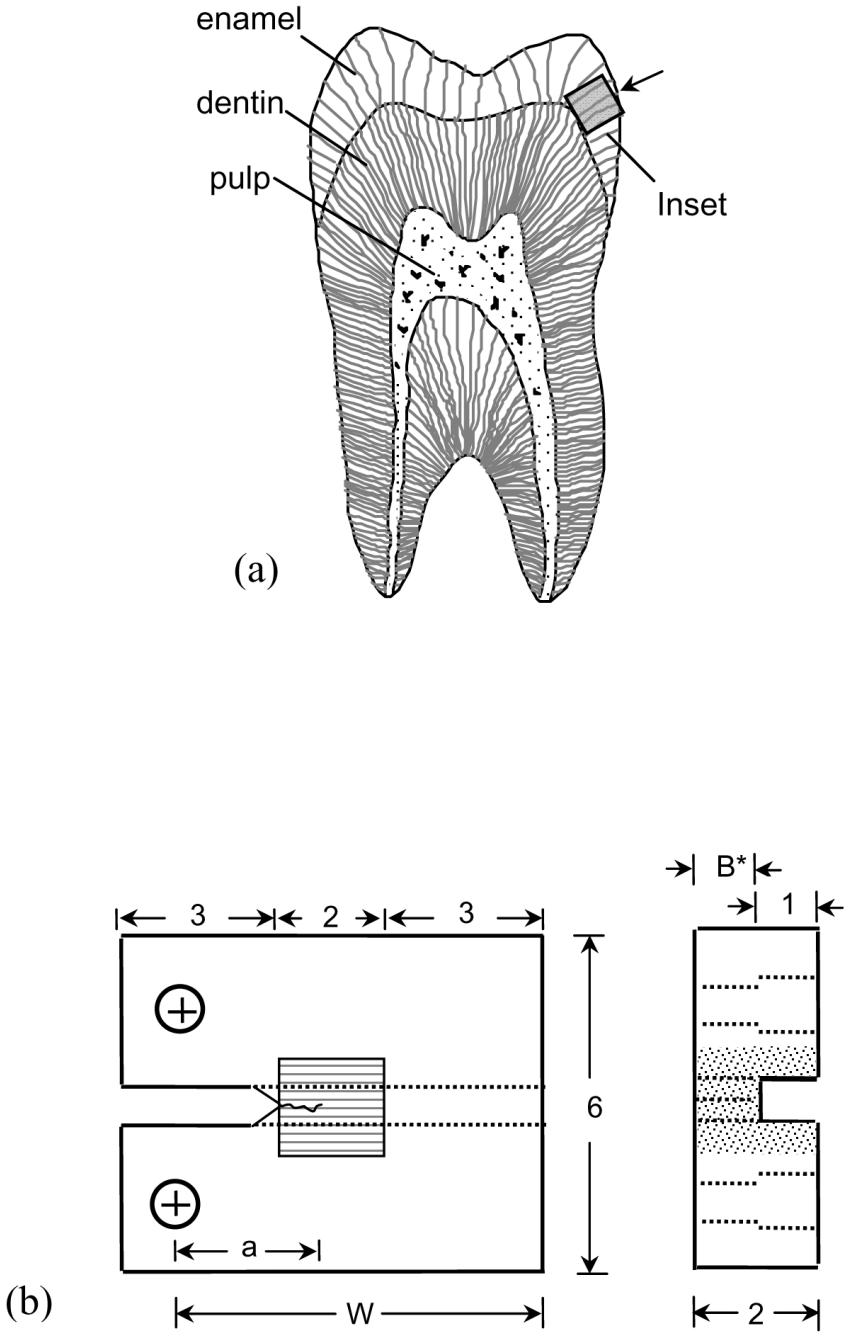

Figure 1.
Details pertaining to the preparation and geometry of the inset CT specimen. (a) A schematic diagram of a sectioned molar highlighting the three different tissues of the human tooth. Also highlighted is a possible section of enamel to be used for the inset. The arrow indicates the direction of crack growth that will be achieved within the inset enamel. (b) Final geometry of the inset enamel CT specimen (all dimensions in mm).

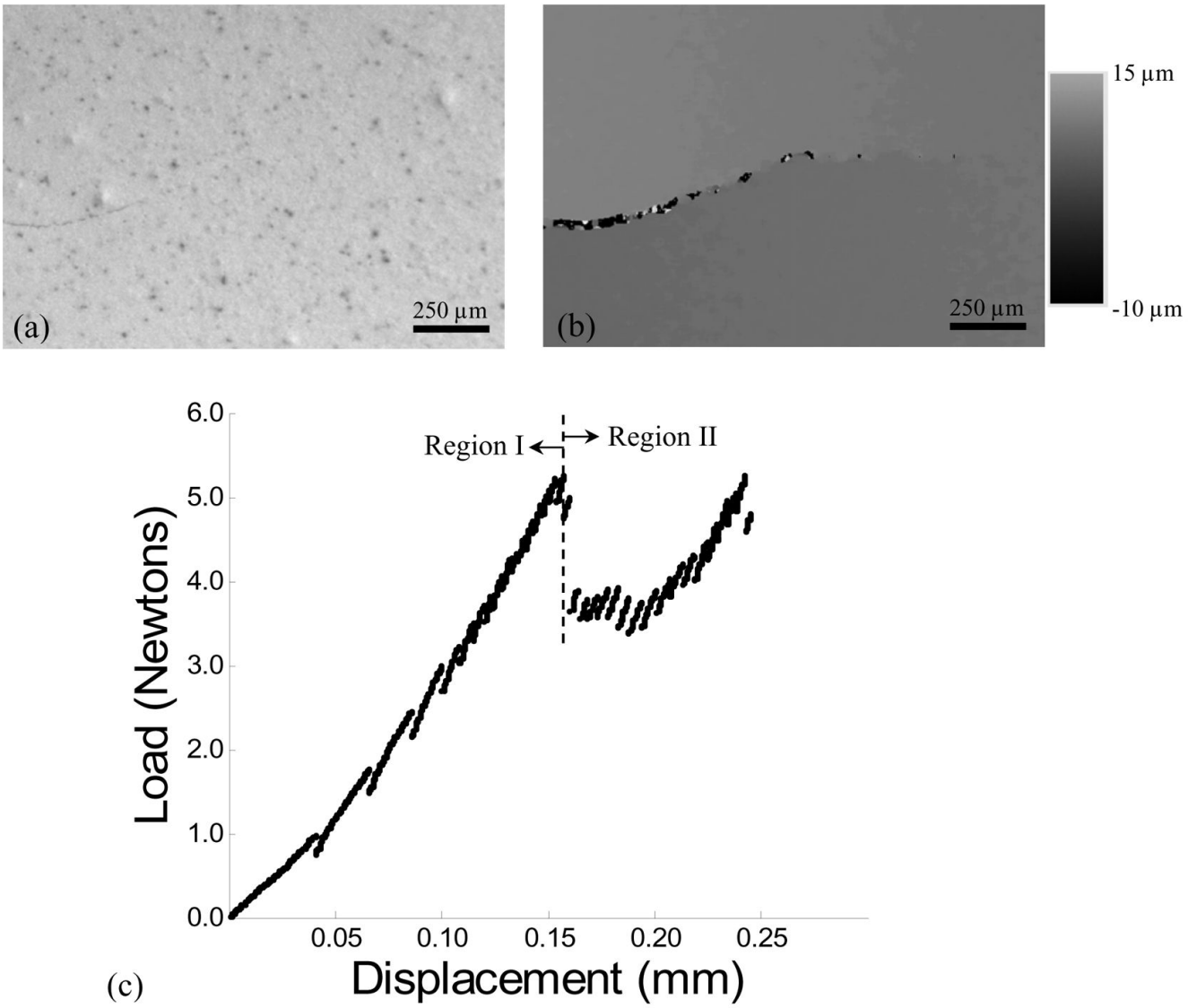

Figure 2.

Details of the experimental evaluation including methods for documenting crack extension and quasi-static loading of the enamel specimens. (a) A digital image of an enamel specimen with stable crack and the "speckle" distribution used in the DIC analysis. (b) An example full field v-displacement distribution about the crack (in (a)) identified using digital image correlation. (c) A load load-line displacement distribution obtained during stable crack extension within an inset enamel specimen. Region I denotes preloading and Region II distinguishes the portion of response associated with incremental crack extension.

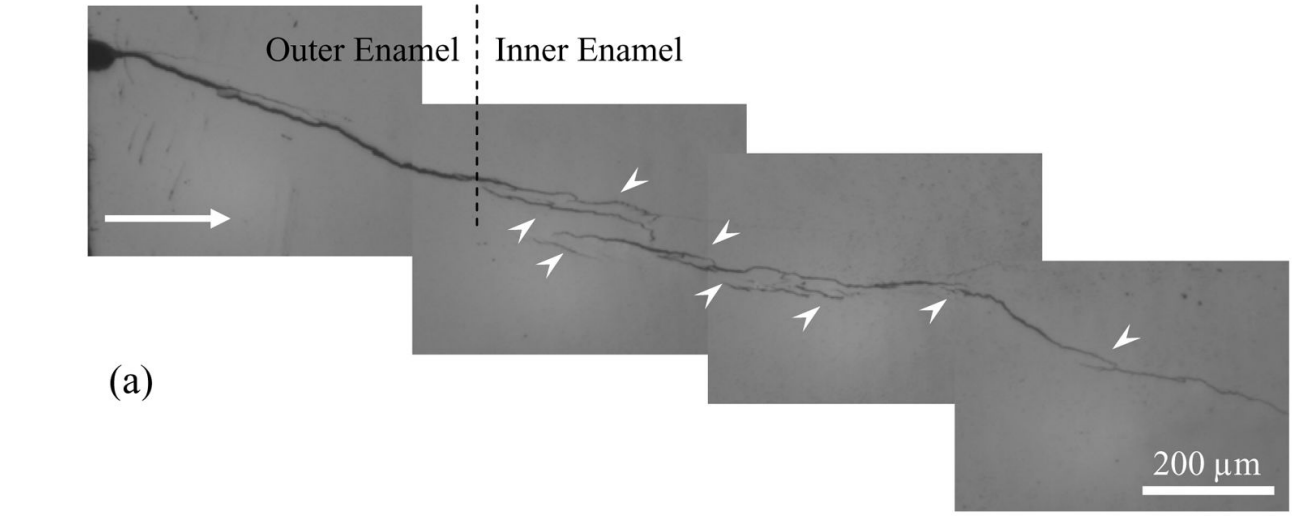

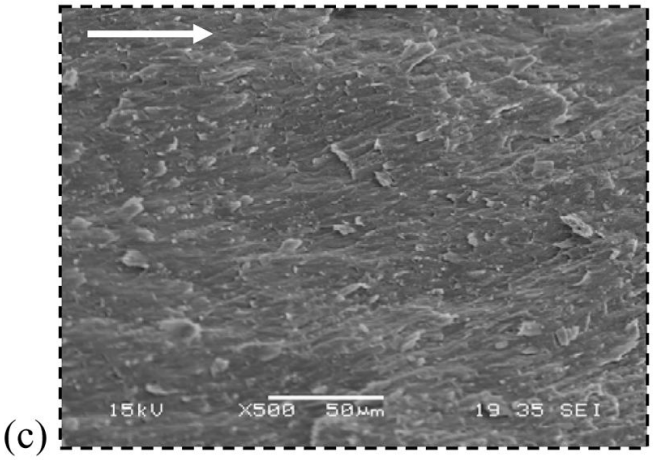

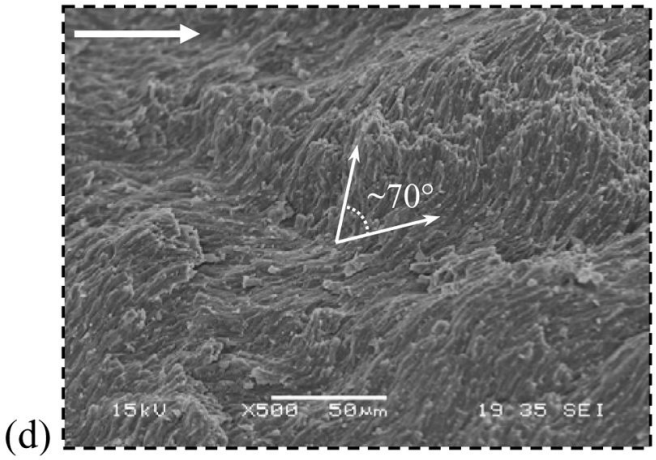

Figure 3.

Observations of crack extension in enamel (crack growth from left to right). The dotted line represents the transition from outer to the inner enamel. (a) An optical micrograph of the crack path in enamel. Crack growth in the outer enamel occurred over a straight path, whereas growth in the inner enamel occurred over a tortuous path accompanied by a number of unbroken ligaments. There was also evidence of crack deflection and crack bifurcation in the inner enamel. (b) A SEM micrograph of a fracture surface. (c) Micrograph of the fracture surface in outer enamel showing a flat fracture plane. (d) Fracture surface in the inner enamel showing tortuous crack plane with evidence of crack deflections up to approximately 70°.

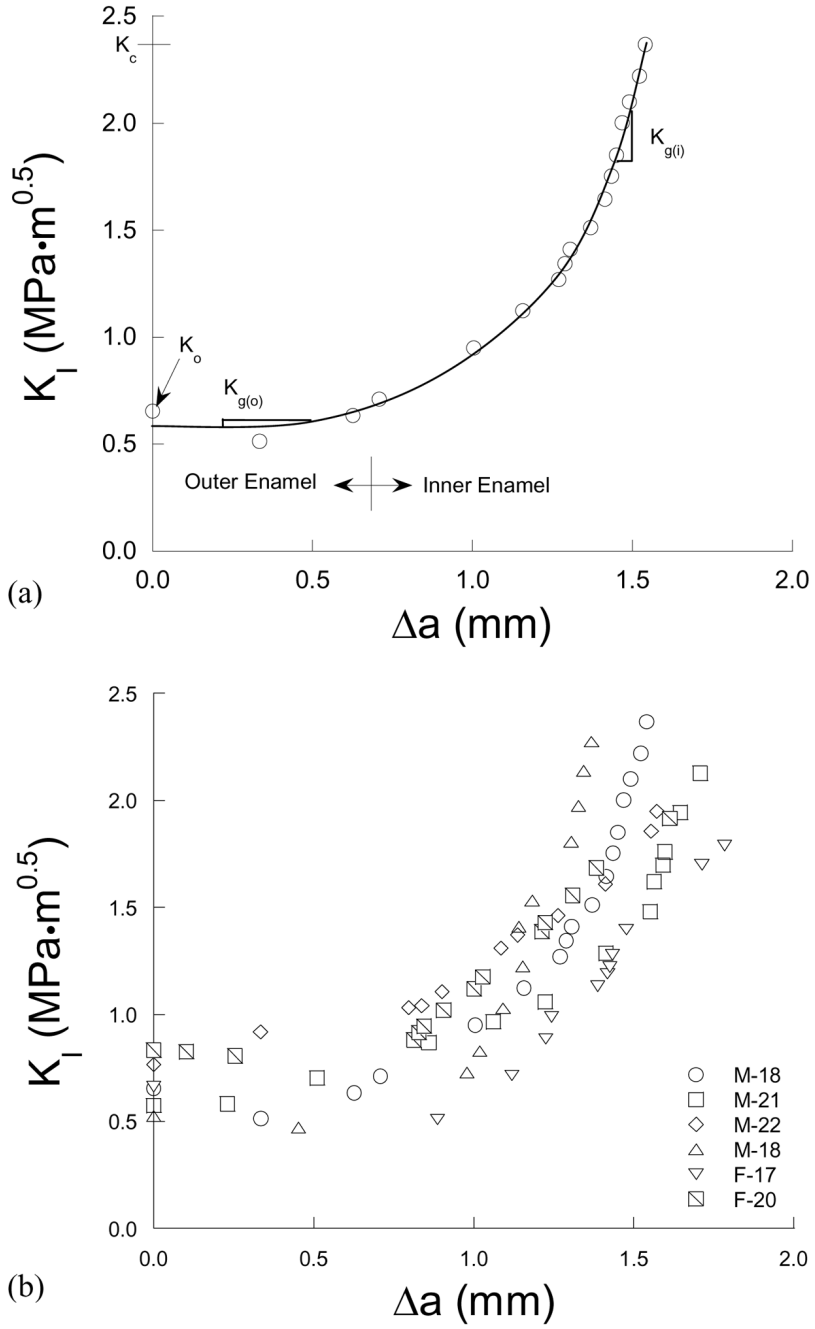

Figure 4.
Crack growth resistance (R-curve) responses for the enamel specimens. (a) A typical resistance curve identifying the specific components of toughness. (b) Results from all the specimens.

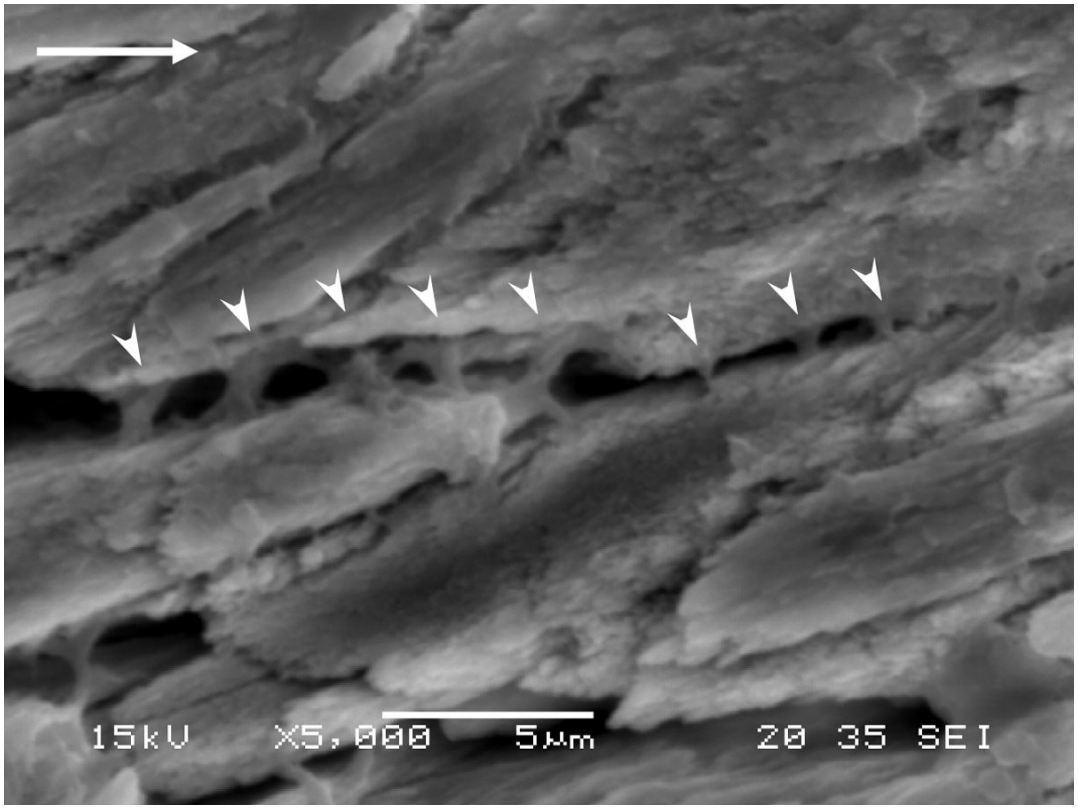

Figure 5.
SEM micrograph of bridging induced by the organic matrix. White arrowheads indicate unbroken ligaments of organic matrix bridging the crack. These bridges were active for crack opening displacements of a few micrometers and result in energy dissipation through extension/unfolding of the proteins.

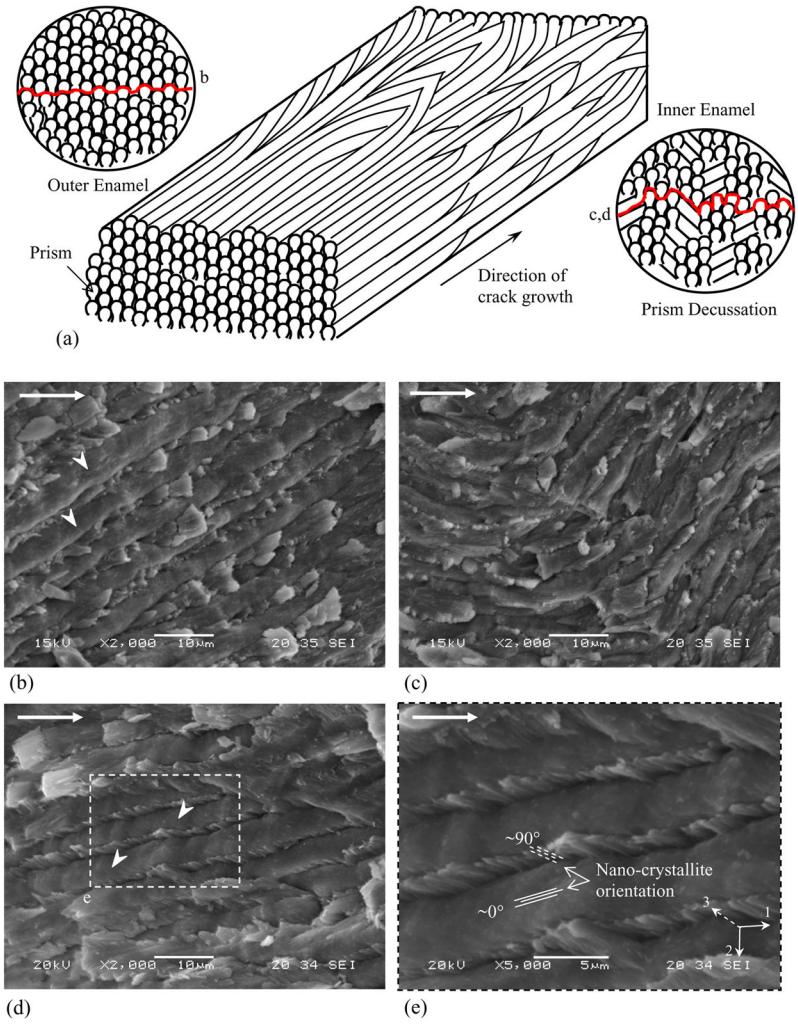

Figure 6.

Observations of the fracture plane within the outer and the inner (decussated) enamel. (a) Schematic diagram of prism orientation in the outer and the inner enamel. Prism curving occurs in the inner enamel resulting in decussation. The inset represents sections perpendicular to the prism axis highlighting the fracture planes and the region where image (b), (c) and (d) were obtained. (b) Crack growth in relatively straight prism orientation occurred along the weak interprismatic spaces. Prism heads (white arrowheads) are evident above the fracture plane. (c) Sharp changes in prism orientation promoted crack deflection and crack twist. (d) Crack growth in decussated enamel required fracture though the prisms and resulted in pullout of the tails. (e) High magnification image of prism fracture indicating the relative orientation of nano-crystallites in the fracture plane.

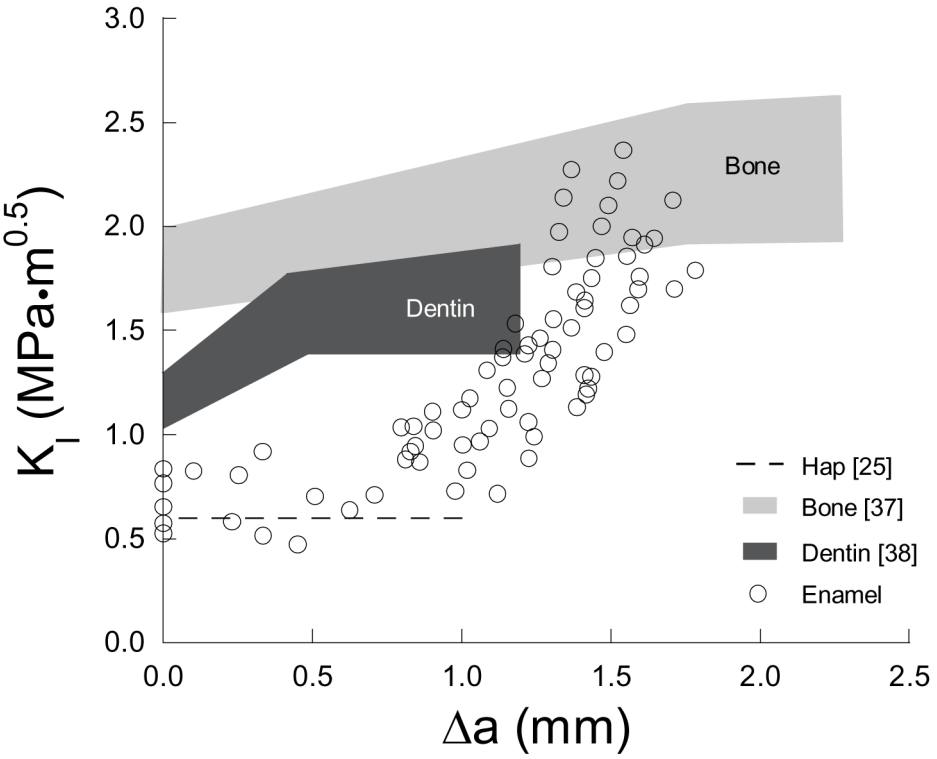

Figure 7.
Comparison of R-curve behavior of enamel with monolithic hydroxyapatite [25], human bone [37] and human dentin [38].

Table 1

Crack growth resistance (R-curve) parameters for enamel.

Gender/Age	Crack Growth Resistance ($MPa \cdot m^{0.5}$)			
		Growth		
	Initiation, K_o ($MPa \cdot m^{0.5}$)	Outer Enamel, $K_{g(o)}$ ($MPa \cdot m^{0.5}/mm$)	Inner enamel, $K_{g(i)}$ ($MPa \cdot m^{0.5}/mm$)	Fracture, K_c ($MPa \cdot m^{0.5}$)
M/18	0.65	−0.04	3.85	2.37
M/21	0.57	0.26	3.93	2.13
M/22	0.77	0.33	1.13	1.95
M/18	0.52	0.22	3.87	2.27
F/17	0.66	−0.01	1.62	1.79
F/20	0.83	−0.11	1.31	1.91
Avg=19±2	0.67±0.12	0.11±0.18	2.62±1.39	2.07±0.22
Pooled	0.68	0.03	1.30	2.04

Table 2

Comparison of crack growth toughness parameters for enamel with other hard tissues such as bone [28,37] and dentin [38].

Toughness Parameters	Enamel	Bone	Dentin
K_o (MPa·m$^{0.5}$)	0.67±0.12	1.84±0.14	1.34±0.06
K_g (MPa·m$^{0.5}$/mm)	2.62±1.39	0.39±0.09	0.93±0.39
K_c (MPa·m$^{0.5}$)	2.07±0.22	2.29±0.25[§]	1.65±0.10

[§] K_C of bone is for crack lengths less than 2.5 mm [37]